3
Materials and methods

Thermal desorption experiments are carried out under ultrahigh-vacuum (UHV) conditions, where the typical gas pressures are of the order of 10^{-10} mbar. Vacuum of this magnitude is a pre-requisite when conducting experiments on the kinetics of adsorption or desorption, because under UHV conditions, the adsorbate layer will be only slightly contaminated by residual gas. Also, only when experiments are conducted under the base pressure mentioned above, a reliable measurement of the increase in gas pressure can be made [Ageev and Ionov, 1975]. In desorption experiments, the increase in gas pressure is often identified as the rate of desorption. The reliable measurement of pressure is therefore crucial for any desorption experiment. The UHV conditions are attained by the proper selection of vacuum components for the chamber and accessories installed inside the chamber, stand-alone bake-out etc. In the first section of this chapter, the main characteristics and components of the UHV system are presented. The maintenance of UHV conditions requires not only a vacuum of 10^{10} mbar to be created, but also needs to be sustained throughout the course of experiments. This often requires stringent sample treatments, which will minimize the outgassing of a sample surface, for example. When using porous carbon materials such as single-wall carbon nanotube bundles, carbon nanofibers etc., this sample pre-treatment is very crucial as under they often adsorb higher concentrations atmospheric contaminants in comparison with crystalline substrates, for instance highly oriented pyrolytic graphite. In addition, these contaminants are found to be more strongly bound to porous materials when compared to crystalline substrates [Ulbricht, 2003]. A detailed description of the sample surface preparation for four carbon surfaces is documented in the subsequent section. Lastly, a section of this chapter is devoted

to experimental methods: thermal desorption spectroscopy (TDS) and temperature programmed oxidation (TPO), where the main principles of these techniques and methods of analysis of data are discussed.

3.1. Experimental setup

In this section, the main features of the experimental setup used for the thermal desorption (TD) experiments are given. This covers a description of the UHV chamber and the vacuum system, the sample holder, the gas dosing system, the temperature and pressure measurement accessories and the data acquisition hard-wares. A complete list of instrumentation is provided in Appendix B.

3.1.1. UHV chamber and vacuum system

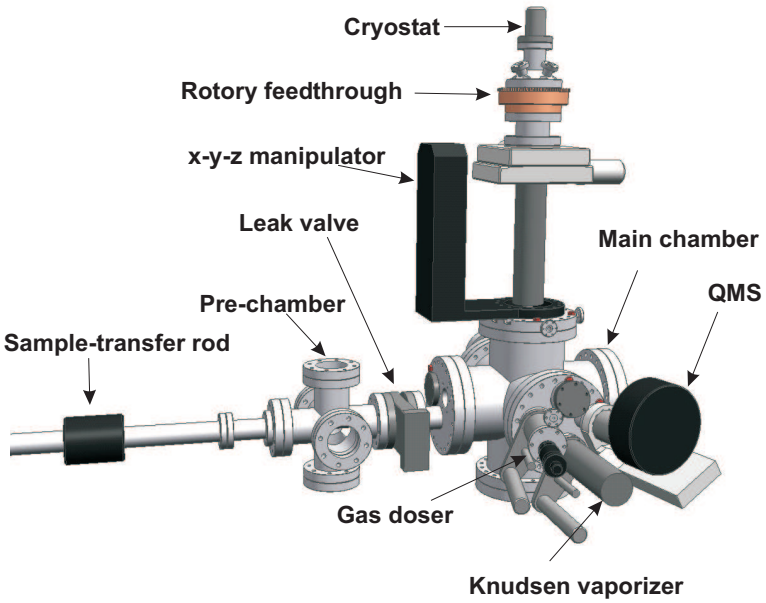

Figure 3.1.: Schematic illustration of the ultrahigh-vacuum chamber and accessories used in the experiments. The pressure, typically around 2×10^{-10} mbar, is maintained within the main chamber. Ionization gauges are on the other side of the chamber and not visible in this illustration.

An overview of the UHV system used for the work reported in this thesis is shown in Fig. 3.1. Two stainless steel subunits, a main chamber and a pre-vacuum chamber, can be identified. They are separated from each other by a manually operated leak valve. The base pressure inside the main chamber is maintained below 2×10^{-10} mbar using a combination of rotary vane pump (Trivac, Leybold), a turbo-drag pump (Hycone 60, Leybold) and a turbo-molecular pump

(Tubrovac 361C, Leybold). Using the combination of a membrane pump (Divac, Leybold) and a turbo-drag pump (Hycone 60, Leybold), a base pressure around 2×10^{-7} mbar is maintained inside the pre-vacuum chamber. The pressure inside both the main and the pre-vacuum chambers are separately monitored using Bayard-Alpert type ionization gauges (Arun microelectronics). After installing a new sample, the UHV chamber and all accessories are typically baked out using a stand-alone bake-out controller and heating module to temperatures between 120 and 150 °C for 24 hours. After cooling to room temperature, this results in a vacuum better than 2×10^{-10} mbar. The residual gas composition inside the main chamber is measured by a quadrepole mass spectrometer (QMS). Typically, the main components in the residual gas are hydrogen ($\sim 65\,\%$), carbon monoxide ($\sim 20\,\%$) and carbon dioxide ($\sim 10\,\%$). The higher mass components are further minimized by degassing the filaments of ionization gauges and mass spectrometer, soon after the bake-out. The components inside the UHV chamber are accessible by means of an x-y-z manipulator (Vakuum Anlagenbau GmbH). A differentially pumped rotational feedthrough allows 360° rotation of the sample around the z-axis.

3.1.2. Sample holder

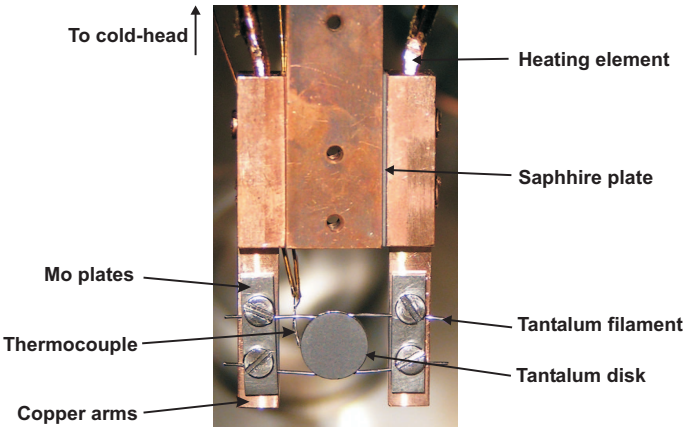

Figure 3.2.: Photograph of all parts in the sample holder assembly. The top of the sample holder is attached to the "cold-head" (not visible in the photograph), a continuous cryogen transport line by which the tantalum disk can be cooled down to ~ 30 K. The temperature of the sample is measured by a K-type thermocouple spot welded to the edge of the tantalum disk.

A photograph of the sample holder used for thermal desorption experiments is shown in Fig. 3.2. The sample holder setup consists of a tantalum disk, approximately 10 mm diameter and 1–2 mm thick, which is centrally located in Fig. 3.2. For thermal desorption experiments, the carbon materials are made into films (see

section 3.2) and fixed on to the tantalum disk. The tantalum disk is supported on two copper arms by a pair of tantalum wires ($\phi = 3$ or 4 mm) and two molybdenum plates. The tantalum wires are fixed to the disk by attaching them on the grooves on the sides of the disk. These tantalum wires also serve as a way to resistively heat the sample surface. The copper arms are electrically isolated from each other by a sapphire plate inserted between one of the copper arms and the main copper body of the sample holder. This arrangement simultaneously provides good thermal coupling between all parts of the sample holder while electrically isolating the heating elements. The sample holder is connected directly to a cold-head, which, through a controlled flow of liquid nitrogen or helium, can be cooled to 77 or 4 K. The temperature of the sample is monitored by a K-type thermocouple spot welded on the side of the tantalum disk. In this arrangement, the sample can be cooled down to ~ 30 K using liquid helium. The heating of the sample is achieved by means of a pair of heating elements attached to two copper arms.

3.1.3. Gas dosing system

The UHV chamber has mounted to it two independent gas dosing systems. One of them is for the exposure of gases and liquids with high vapor pressures. This dosing system consists of several gas-inlets which are connected to a constant width orifice and passes through a gas reservoir and leak valves. The orifice is a part of the King-Wells type of dosing setup, and has a stainless steel tube of roughly 200 mm length and a 10 µm pinhole. This setup provides a controlled molecular flow of gases to the sample surface [King and Wells, 1972]. The gas inlets are connected to high purity laboratory gases (Messer GmbH). Before each dosing, the reservoir is purged to ensure high gas purity. The gas pressure within the reservoir is measured using a capacitance-type Pirani pressure gauge. To dose liquids, an additional reservoir is provided. When dosing liquids, the dissolved atmospheric impurities are pumped out using freeze-pump-thaw cycles. For hydrogen peroxide, additional care has been taken to minimize the amount of time the gas is left inside the reservoir, this avoids decomposition of peroxide within the reservoir. Additionally, the peroxide temperature is normally kept below room temperature, to hinder its thermal decomposition. A gas flux on the order of $10^{11}\,\mathrm{mol\,s^{-1}\,cm^{-2}}$, or about $0.01\,\mathrm{ML\,s^{-1}}$ can be released onto the surface by using a pressure of 1 mbar in the gas reservoir (this flux corresponds to the exposure of Xe). The second dosing set up is used for the sublimation of low vapor pressure solid materials, such as polyaromatic hydrocarbons. This dosing system is a series of Kundsen cells which can be heated to a desired temperature using a proportional-integral-differential controlled programmable power-supply system, and is provided with a cooling water-jacket. The sample is accessible to the various dosing stages mentioned above by means of an x-y-z manipulator and a 360° differentially pumped rotational feedthrough.

3.1.4. Temperature measurement and control

Temperature control of the experiment allows for the sample to be scanned between $\sim$30 to 1200 K. Cooling down of the sample to 30 K is possible by continuous supply of a liquid cryogen (nitrogen or helium) through a transport line (Janis ST-400) and cryogen feedstock. The temperature of the sample surface is measured using a K-type thermocouple spot welded to the edge of the tantalum disk and is calibrated using the Xe multilayer desorption peak from graphite surface [Ulbricht, 2003]. The sample surface is heated resistively using two heating elements which are fixed on the copper arms of the sample holder. They are connected to a programmable power-supply system (Delta Electronika SM 35-45) and a temperature controller (Lakeshore 340). For thermal desorption experiments, temperature is varied in a linear fashion with heating rates between $0.5\,\mathrm{K\,s^{-1}}$ and $2\,\mathrm{K\,s^{-1}}$, which is programmed using temperature controller. Temperature measurement is acquired by a PC through a GPIB (general purpose interface bus) connector.

3.1.5. Pressure and desorption rate measurement

As will be discussed later in this chapter, the desorption rate can be monitored by directly recording the pressure inside the chamber, under high pumping speed (S), i.e., $\Delta p \propto dN/dt$ [Eq. (3.4)]. The pressure inside the UHV chamber is monitored using Bayard-Alpert ionization gauges and an ionization gauge controller (Arun microelectronics). However, the use of an ionization gauge to monitor the desorption rate is reliable only when the adsorbent purity is ensured. Also, credible measurements of desorption rates using ionization gauges can be done only if there are no chemical transformations during desorption, for example as seen during the thermal desorption of polyaromatic hydrocarbons from graphite. In order to gain confidence in performing a desorption experiment using ionization gauges, the thermal spectra of the residual gases inside the chamber are recorded and are used for the TD spectra background correction. The pressure measurement is accessed to a PC through an RS-232 connection.

The continuous monitoring of gas compositions is also possible with mass spectroscopic techniques. They are preferred due to their extremely high sensitivity and high resolution. The use of a mass spectrometer allows the determination of partial gas pressures, where the flux intensity of desorbing molecules is proportional to the ion current recorded by the mass spectrometer. In these experiments, the partial pressures of various desorbing gases are monitored using a quadrepole mass spectrometer (LedaMass, Satellite 220 D). This setup can simultaneously scan for multiple species with charge-to-mass ratio of up to 200 a.m.u./e. Also, the quadrepole mass spectrometer is used to make residual gas analysis prior to exposing the sample surface to gas molecules. The measurement of partial pressures is interfaced to a PC through a RS-232 connector.

3.1.6. Data acquisition

All experimental data are acquired on a PC (PIII, 1 GHz) using specialized hardware, such as GPIB and multifunction data acquisition cards (PCI-MIO 16-E4, National Instruments). Data acquisition programmes are controlled by LabVIEW 6i and NiDAQ (National Instruments). Pressure and temperature measurements from the quadrepole mass spectrometer, ionization gauge controller and temperature controllers are interfaced with software (LabVIEW 6i) using either IEEE-488 and RS-232 interfaces, and GPIB and PCI-MIO (National Instruments) data acquisition hardware.

3.2. Sample preparation

In this section, I will present a brief discussion of the characteristics of four carbon materials: highly oriented pyrolytic graphite (HOPG), single-wall carbon nanotube bundles (SWNTs), carbon nanofibers (CNFs) and colloidal graphite (CG), and experimental methods adopted for the sample surface preparation.

3.2.1. Graphite

Thermal desorption experiments from graphite are performed using synthetic graphite, also known as highly oriented pyrolytic graphite (Grade ZYB, Advanced Ceramics). These samples are typically produced by the pyrolytic decomposition of carbonaceous vapors, where under suitably controlled conditions (i.e., temperature of $\sim 3000\,^{\circ}\mathrm{C}$ and pressure of ~ 400 atmospheres), the deposits take the form of highly oriented basal layers. Often synthetic routes produce large slabs of pure and perfect graphite crystals [Reynolds, 1968]. The name, highly oriented pyrolytic graphite refers to the high degree of mutual orientation observed in graphene basal planes. The microscopic examination of a single HOPG crystal reveals that it consists of small crystallites having a few tens of nanometers in dimension, with basal planes stacked along (001)-orientation [Ohler et al., 1997] (details of graphite lattice structure is provided in section 4.1).

For desorption experiments, the HOPG sample ($12\,\mathrm{mm} \times 12\,\mathrm{mm} \times 1\,\mathrm{mm}$) is cut into a dimension to match that of the tantalum disk, (see sample holder, Fig. 3.2) and is affixed to the disk using a conducting silver epoxy. A typical HOPG sample used for experiment has a thickness of few tenths of a millimeter and a diameter of roughly 10 mm. The sample surface is cleaved using an adhesive tape, just before the transfer into vacuum chamber. Once the sample is mounted inside the chamber, the surface is outgassed by repeated annealing at 1100 K. The prominent surface contaminants, as indicated by rest gas analysis, are water and chemisorbed oxygen. They are minimized by the repeated annealing at high temperatures.

3.2.2. Single-wall carbon nanotube bundles

Single-wall carbon nanotubes are a hexagonal network of carbon atoms with a seamless, hollow, cylindrical geometry, and have unique electronic, mechanical and surface properties [Iijima, 1991]. They possess intriguing surface properties, especially adsorption, wetting and binding with external molecules, due to the interaction of all surface atoms with the external environment [Hertel, 2003; Ulbricht et al., 2004]. Single-wall carbon nanotubes exhibit properties which are strongly dependent on their structure. As mentioned above, their structure derives from rolling up a single graphene sheet. Since there are infinitely many ways of rolling up a graphene sheet, the tubes are defined by their diameter and chiral angle. The chiral angle is defined as the angle of the hexagonal helix around the tube axis. As explained in the following, the rolled up graphene units are classified based on their structure, into three groups: "zig-zag", "arm-chair" and "chiral" carbon nanotubes (Fig. 3.3). Due to their close similarity with graphene sheets, the above three classes are defined by graphene lattice vectors of graphite unit cell $\mathbf{a}_1$ and $\mathbf{a}_2$ [Fig. 3.3(a)]. In carbon nanotubes, a graphene sheet is rolled up in such a way that a vector $\mathbf{c}$ ($\mathbf{c} = n\ \mathbf{a}_1 + m\ \mathbf{a}_2$), where n and m are integers, becomes the circumference of the tube. The direction of this circumferential vector, called chiral vector, can be measured by chiral angle θ, which is defined as the angle between $\mathbf{a}_1$ and $\mathbf{c}$. It is calculated using [Dresselhaus and Avouris, 2001]:

$$\cos\theta = \frac{\mathbf{a_1} \cdot \mathbf{c}}{\mid \mathbf{a_1} \mid \cdot \mid \mathbf{c} \mid}. \tag{3.1}$$

Above three classes of nanotubes, zig-zag, arm-chair and chiral carbon nanotubes, are differentiated using this chiral angle. Tubes of type $(n, 0)(\theta = 0^\circ)$ are zig-zag tubes because they exhibit a zig-zag pattern of carbon atoms along the circumference. An example of this type of SWNT is a (7,0) tube, where $n = 7$ and $m = 0$ and $\theta = 0^\circ$ [Fig. 3.3(b)]. Arm-chair tubes have chiral vectors of type (n, n) and chiral angle of $\theta = 30^\circ$. An example of this type of tube is a (4,4) tube, with m and $n = 4$ [Fig. 3.3(c)]. Lastly, tubes with any arbitrary combinations of chiral vectors as represented by a chiral vector $(5, 3)$ in Fig. 3.3(d), is a chiral tube. The properties, in particular the electronic properties, of SWNTs are found to be a strong function of structure. For instance, all zig-zag and chiral tubes are semiconducting while all arm-chair tubes are metallic [Louie, 2001]. The structural influence on the surface properties is, however, unknown at present.

Single-wall carbon nanotubes used in these experiments are either synthesized by the laser ablation method which are obtained from Rice University (Tubes@Rice), or are produced by high pressure CO conversion (HiPCO) from CNI, Houston [Nikolaev et al., 1999; Thess et al., 1996]. Laser ablation material generally contains more than 90 % single-wall carbon nanotubes. Other components commonly observed are graphitic materials, fullerenes etc. The second method produces material with more than 98 % purity. The samples used in our experiments have a mean

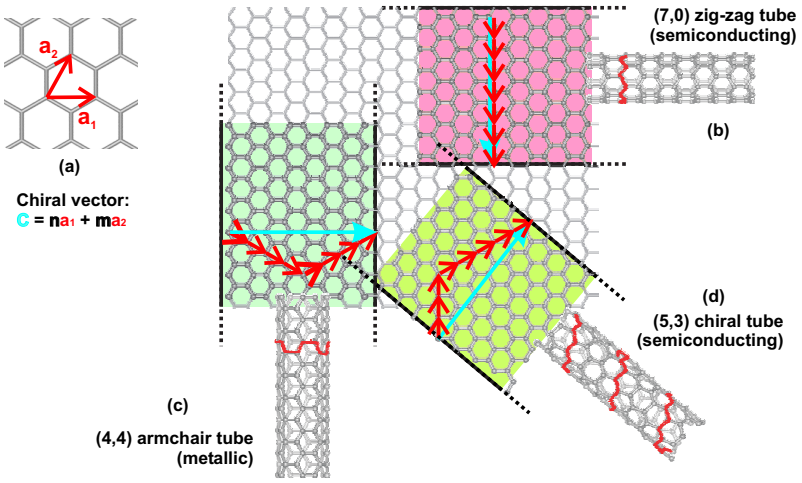

Figure 3.3.: (a) Lattice vectors $\mathbf{a}_1$ and $\mathbf{a}_2$ of a graphene sheet. By rolling up the graphene sheet along the zig-zag and the arm-chair or along any other directions in between these two, generates (b) a zig-zag tube, (c) an arm-chair tube or (d) a chiral carbon nanotube, respectively. Above three classes of nanotubes can be distinguished by their chiral vector, $\mathbf{c}$, which is related to the lattice vectors of graphene sheet by $\mathbf{c} = n\ \mathbf{a}_2 + m\ \mathbf{a}_2$. Here, n and m are integers which represent indices of a carbon nanotube.

diameter of around 1.2 nm (for laser ablation sample) or 1.0 nm (for HiPCO sample). They are typically available as an aqueous suspension or as a black powdery material, each of which is used to prepare a film of nanotubes. In preparing this "bucky paper", I use a procedure introduced by Rinzler et al. [1998]. This method uses a uniform suspension of nanotube in tri-distilled water, which is prepared by ultra-sonication. The solution is vacuum filtered through a polycarbonate membrane filter paper (0.5 µm pore size, Millipore). The filter-cake, together with the polycarbonate membrane, is desiccated by vacuum annealing to 200 °C for typically one hour. The bucky paper is then separated from the polycarbonate membrane filter and used for thermal desorption experiments. The density of a typical bucky paper sample is $0.6\,\mathrm{g\,cm^{-3}}$. From a comparison of this sample density with that of a closely packed nanotube bundle ($1.5\,\mathrm{g\,cm^{-3}}$), it is found that nearly 60 % of the sample is void or pores. Microscopic studies of similar bucky papers revealed a "spaghetti-like" structure [Fig. 3.4(a)] [Rinzler et al., 1998]. A closer examination of this rope-like structure shows that it consists of several single-walled nanotubes, which are formed by the agglomeration of individual tubes into a quasi-crystalline hexagonal structure [Fig. 3.4(b)]. The wall-to-wall distance between two tubes is in the same range as the interlayer distance in graphite (3.41 Å). This clearly indicates that the self-assembly in SWNT bundles is due to strong van der Waals interactions, analogous to that in graphite. Care has been taken to prepare a thin film, so as to minimize the temperature gradient across the film thickness. The dried film is

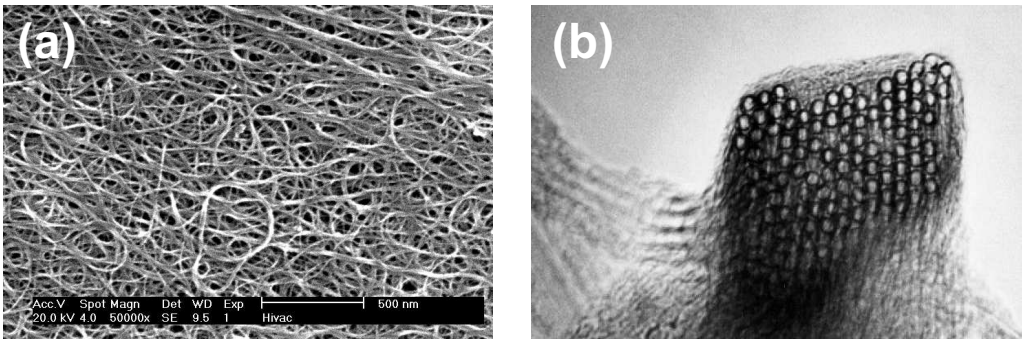

Figure 3.4.: The structural details of a buck paper. (a) SEM figure of a typical sample shows spaghetti-like structure with large void regions. (b) A closer examination using TEM, reveals that each rope like feature is an agglomeration of several single-wall carbon nanotubes, which has a quasi-crystalline hexagonal close-packed structure. Figures are adapted from www.http://cnst.rice.edu/pics.html

spread on the tantalum disk, and is made to adhere to the disk by wetting the film with a drop of ethanol. Excess solvent is allowed to vaporize. The tantalum disk, along with the bucky paper, is mounted inside the UHV chamber. The sample surface is cleaned by repeated annealing at 1100 K and is used for the thermal desorption experiments. The main contaminants on bucky paper are found to be oxides of carbon, water and chemisorbed oxygen species, which are outgassed by repeated heating at 1100 K.

3.2.3. Carbon nanofibers

Carbon nanofibers (also known as carbon nanofilaments) represent an important class of graphite related materials, which are closely related to carbon nanotubes in regard to their structure and properties [Louie, 2001]. However, they show superior catalytic properties in comparison to carbon nanotubes or similar graphitic materials [Maximova, 2002; Ros, 2002]. They are typically synthesized by the catalytic decomposition of carbon containing gases on catalytic metal particles. Carbon nanofibers produced by this vapor deposition are found to be generally pure and free of other carbonaceous deposits such as, 'onion-like' or amorphous carbons. Using a reaction temperature between 400 and 900 °C, fibers of diameter 10–100 nm and lengths up to 1000 µm are obtained [Ros, 2002]. Depending on the structure, carbon nanofibers are classified into two groups: parallel and fish-bone nanofibers. Parallel nanofibers consist of coaxial cylindrical sheets of carbon, in which graphitic layers are oriented parallel to the fiber axis. Structure-wise, the parallel fibers are similar to multi-wall carbon nanotubes. Fish-bone types of nanofibers have 'cone-shaped' graphitic layers and are stacked on top of each other. Figure 3.5(a) shows a schematic illustration

of parallel and fish-bone carbon nanofibers. The surface of parallel fibers consists of

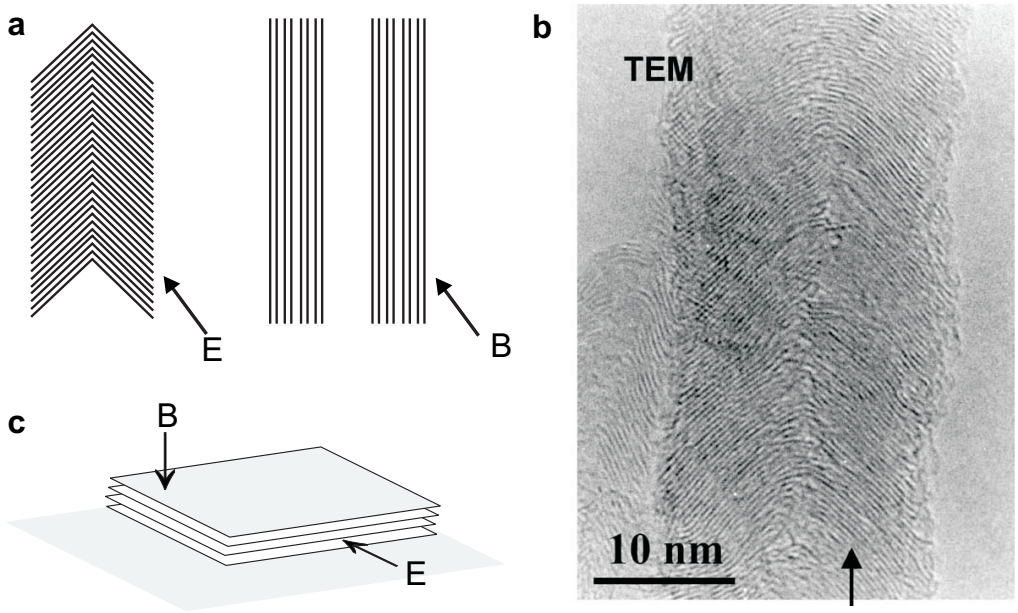

Figure 3.5.: Schematic illustration and TEM image of carbon nanofibers. (a) The carbon nanofibers are classified into fish-bone or parallel depending on their structure. Fish-bone carbon nanofibers (b) have 'cone-shaped' graphitic layers stacked on top of each other as evident from the TEM micrograph. The parallel nanofibers have their cylindrical graphitic layers coaxially arranged. (c) Schematic illustration of the reactive edge (E) and basal (B) planes of the graphitic carbon materials. TEM micrograph is adapted from Ledoux et al. [2003].

a high density of basal planes, while the surface of fish-bone carbon nanofibers has greater density of edge planes. The superior catalytic activity of the fish-bone carbon nanofibers is explained in terms of this surface structure (i.e., the basal versus edge plane). The activation and dissociation of oxygen molecules happen readily on the surface of the fish-bone carbon surface in comparison to other graphitic carbon surfaces, for example. The specific surface area of these fibers determined using Brunauer-Emmett-Teller (BET) method indicates a value in the range of 100 to $200\,m^2\,g^{-1}$ [Ros, 2002]. Since the fish-bone nanofibers are surface terminated with the more reactive edge planes, they are susceptible to modification to form surface functional groups very similar to those in organic chemistry [Maximova, 2002; Ros, 2002]. Therefore, the carbon nanofibers used in these studies are only the fish-bone type of carbon nanofibers. Experiments are performed with the samples obtained from Applied Science Inc., Cedarville, USA. The material, as supplied by the Applied Science, is used without further purification. The black powdery material is made into a uniform aqueous suspension by ultra-sonicating approximately 0.01 mg

in 100 ml of tri-distilled water. The solution is spray coated on the tantalum disk, and concurrently the disk is resistive-dried to remove the solvent. After spray coating, the sample is mounted inside the UHV chamber. The sample is repeatedly outgassed by heating to 1100 K, till the desorption from chemisorbed species such as water, carbon oxides and oxygen has reached minimum.

3.2.4. Colloidal graphite

Colloidal graphite, which is a colloidal dispersion of graphitic crystallites in aqueous medium, is obtained from Agar Scientific (Essex, England). The colloidal suspension is stabilized against precipitation by additives, which generally evaporate upon mild heating. In aqueous media colloidal graphite appears as a black suspension which undergoes fast sedimentation. Sedimentation is avoided during spray coating by continuous agitation of the dispersion. A thin and uniform film of colloidal graphite is made by spray coating the aqueous suspension on to the tantalum disk. The sample is outgassed after mounting it inside the UHV chamber as described previously.

3.3. Temperature programmed desorption

One of principle methods for the experimental determination of kinetic and energetic parameters of adsorption and desorption is thermal desorption spectroscopy (TDS). Historically, this technique evolved out of *flash filament desorption*, a method proposed by Becker and Hartman [1953] and also known as temperature programmed desorption (TPD). In this section, I present the fundamentals of the TDS method and two methods of analysis for TDS data. Due to the availability of excellent reviews and monographs on this topic, a detailed presentation is not attempted here [Ageev and Ionov, 1975; Christmann, 1991; King, 1975; Redhead, 1962].

3.3.1. Principles

The experimental aspects of thermal desorption spectroscopy are based on the concepts of adsorption and desorption. If a solid with a surface free of adsorbed particles is placed in a gas medium, the process of adsorption will commence. Under static conditions, this process will continue in static until an equilibrium concentration of adsorbed particles is reached. If the solid surface under consideration is placed inside in a chamber of volume (V), which is under a constant evacuation at speed S, and the gas is leaked at a constant rate (L), the above equilibrium concentration can be described in terms of the steady-state pressure (p_{eq}) inside the chamber:

$$L = KSp_{eq}. \tag{3.2}$$

Here K represents the proportionality constant ($K = 3.27 \times 10^{19}\,\text{molecules}\,\text{l}^{-1}$, at $p = 1\,\text{torr}$ and $T = 295\,\text{K}$). If the sample surface is heated at a constant rate, the gas pressure inside the chamber increases due to the flux of desorbing particles. Assuming no re-adsorption of the desorbing particles, the mass balance of particles leaving and entering the chamber is given by adsorption and desorption processes:

$$A\frac{dN}{dt} + L = KSp + KV\frac{dp}{dt}, \tag{3.3}$$

where, A is the surface area of the adsorbent, dN/dt is the net flow rate (rate of desorption) and p is the instantaneous pressure inside the chamber. Note, in the above formulation, adsorption on the walls of the system has also been disregarded. Using Eq. (3.2), and substituting Δp for $p - p_{eq}$, the equation of mass balance [Eq. (3.3)] can be simplified as

$$\frac{d\Delta p}{dt} + \frac{\Delta p}{\tau} = a\frac{dN}{dt}. \tag{3.4}$$

Here $a = A/KV$ and $\tau = V/S$. τ is the characteristic pumping time. Depending on

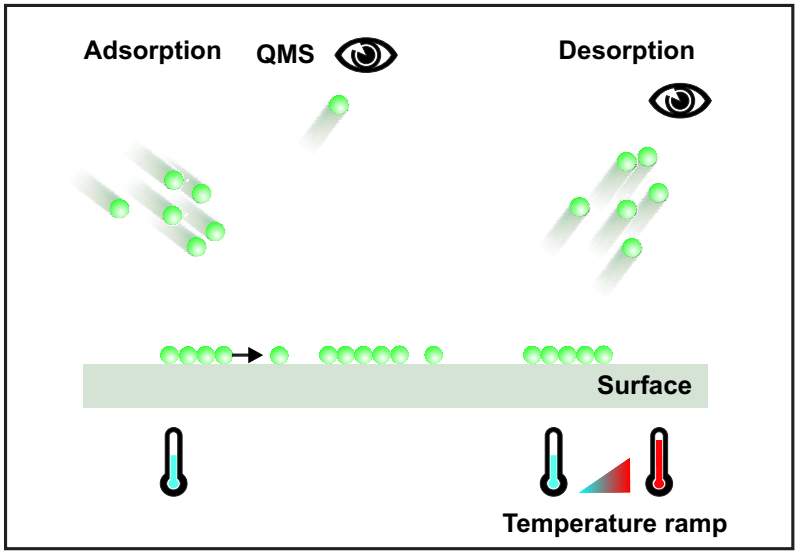

Figure 3.6.: Illustration of processes during temperature programmed desorption. As shown on the left side, the exposure of the surface to a molecular beam of gases results in the formation of mono- and multilayers by physisorption or chemisorption. The exposure is typically conducted at low temperatures (30–100 K), since the binding energies for physisorbed species are of the order of few hundred meVs. The desorption as shown on the right side, is carried out by heating the sample surface in a linear fashion and the desorbing molecules are monitored using a quadrepole mass spectrometer.

the magnitude of the pumping speed, two experimental scenarios can be identified

here: (1) at a small pumping speed ($\tau \rightarrow \infty$), the desorption rate is proportional to the first derivative of pressure with time ($dN/dt \propto d\Delta p/dt$). Alternatively, at high pumping speed ($\tau \rightarrow 0$), desorption rate is proportional to the pressure ($\Delta p = a\ \tau\ dN/dt$). Experiments described in this thesis are performed under a high pumping speed. During desorption, the temperature of the sample surface is controlled in a linear fashion, i.e, $T = T_0 + \beta t$, T_0 is the initial sample temperature and β is the heating rate dT/dt. The determination of various adsorption and desorption parameters, such as: (a) number and population of various desorbing phases, (b) activation energy of desorption, (c) the order of the desorption and (d) the pre-exponential frequency factor for the desorption, by thermal desorption spectroscopy is based on the analysis of the pressure-temperature curve (referred to as desorption spectrum). The methods of analysis of desorption spectra are discussed later in the chapter.

3.3.2. Temperature programmed oxidation

Temperature programmed oxidation (TPO) is a variant of the temperature programmed techniques, where the solid surface under study is exposed to oxidizing agents and different temperatures [Bhatia et al., 1990]. It is generally applied in combination with desorption experiments and yields information about redox properties of metal and metal-oxide catalysts: the characterization of the coke species in the deactivated catalysts; the total coke content in the deactivated catalysts and mechanism and kinetics of oxidation reactions [Kanervo, 2003]. For this thesis, TPO was carried out by oxidizing the carbon surfaces using exposure to hydrogen peroxide under various conditions of pressures and surface temperatures. The desorbed species from oxidized surfaces are monitored, similar to normal desorption experiments, and desorption traces are analyzed using aforementioned techniques.

3.3.3. Analysis of TDS data

Analysis of desorption traces is based on treating the desorption process as a kinetic phenomenon. The equilibrium of a surface species in contact with its gas phase component can be represented as:

$$[A]_s \rightleftharpoons [A]_g, \tag{3.5}$$

where $[A]_s$ and $[A]_g$ are the surface and the gas phase concentrations of an adsorbent molecule, A. The rate of desorption of adsorbed molecules from the surface is then given by:

$$-\frac{dA}{dt} = k[A]^n, \tag{3.6}$$

where n is the order of the desorption and k is the rate constant for the desorption. The rate constant k has a temperature (T) dependence and is given by Arrhenius

equation,

$$k = \nu \exp\left(-\frac{E_d}{k_B T}\right). \tag{3.7}$$

Here, ν is the pre-exponential frequency factor, E_d is the activation energy of desorption and k_B is the Boltzmann constant. In thermal desorption analysis, the surface concentration of adsorbents ($[A]_s$) is conventionally expressed as 'σ' or 'θ', where σ is the number of particles adsorbed per unit area of the adsorbent, and θ is the surface concentration expressed in units of monolayers (MLs), i.e., most close-packed arrangement of adsorbed particles on the adsorbent. Using the above substitutions, Eq. (3.6) can be rewritten as:

$$-\frac{d\theta}{dt} = \nu \theta^n \exp\left(-\frac{E_d}{k_B T}\right). \tag{3.8}$$

A typical thermal desorption spectrum of ethylbenzene (C_8H_{10}) from highly oriented pyrolytic graphite with features corresponding to the physisorption is displayed in the Fig. 3.7. The spectrum is obtained by exposing the HOPG surface to an exposure of 1.1 L (1 Langmuir = 1×10^{-6} Torr s), and a heating rate of $1\,\mathrm{K\,s^{-1}}$. A desorption spectrum corresponding to the physisorption of gas molecules is characterized by a number of desorption peaks, which is caused by the desorption of various adsorbed phases. The temperature ranges at which desorption peaks appear indicate the nature of adsorption, i.e., physisorption or chemisorption. For example, physisorbed phases have desorption peaks generally at lower temperatures ($< 400\,\mathrm{K}$), while chemisorbed species generally desorb at higher temperatures ($> 600\,\mathrm{K}$). In a typical desorption spectrum from a physisorbed species, it is possible to identify the desorption features originating from the first monolayer, the second monolayer and multilayers. As shown in the above TD spectrum of ethylbenzene, the desorption peak at 209 K corresponds to desorption from the first monolayer. Desorption from the multilayers appears at lower temperatures, as shown in Fig. 3.7, where the peak corresponding to multilayer desorption appears at 171 K. Determination of adsorption and desorption parameters from TD traces, such as in Fig. 3.7, can be done using various methods, i.e., Redhead analysis, complete analysis etc., each having its own merits and demerits [de Jong and Niemantsverdriet, 1990]. The TD traces reported in this thesis are analyzed using both the peak maximum method introduced by Redhead [1962] and the Falconer-Madix method [Falconer and Madix, 1977].

Use of the peak maximum method is based on an approximate solution of Arrhenius equation, which linearly relates activation energy of desorption with T_{max}, the temperature of the maximum desorption rate. For first-order desorption ($n = 1$), Redhead has shown that the Arrhenius equation can be solved to obtain

$$E_d/k_B T_{max}^2 = (\nu/\beta) \exp\left(-E_d/k_B T_{max}\right). \tag{3.9}$$

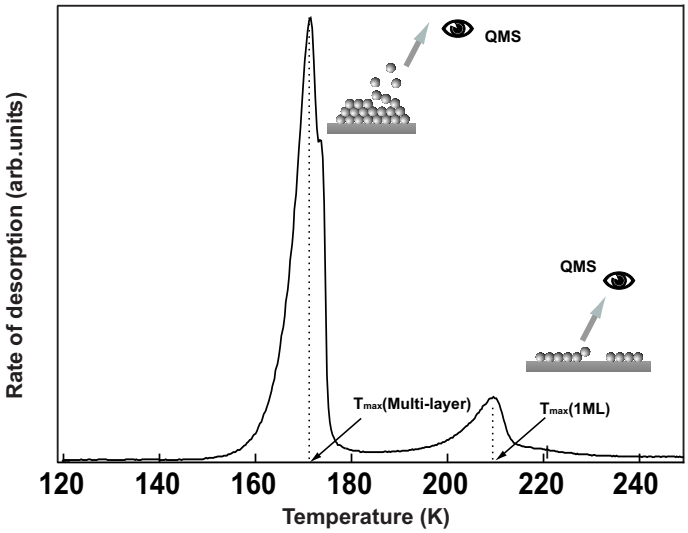

Figure 3.7.: Thermal desorption spectrum of ethylbenzene from the surface of highly oriented pyrolytic graphite obtained by an exposure of 1.1 L and a heating rate of $1\,\mathrm{K\,s^{-1}}$. The TD spectrum is obtained by plotting the signal corresponding to the partial pressure of ethylbenzene versus temperature. The peak that appears at 209 K is due to the desorption of ethylbenzene from the first monolayer. Desorption from typical multilayers appears at lower temperatures and is a function of exposure. Here, the peak that appears at 171 K is attributed to the desorption from the multilayers. Each desorption peak is characterized by a temperature (T_{max}), where the rate of desorption reaches its maximum. The initial surface coverage can be obtained from the area under the TD spectrum. T_{max}, corresponding rate and surface coverages are then used to evaluate a series of TD spectra and to calculate various desorption parameters.

Using the above relation, the following linear relation between E and T_{max} can be shown:

$$E_d = k_B T_{max}[\ln(\nu T_{max}/\beta) - 3.64]. \tag{3.10}$$

The use of this 'Redhead equation' to derive the activation energy is generally valid for first-order desorption. However, it can be successfully extended to the evaluation of thermal desorption spectra corresponding to a different desorption order, if the T_{max} used is obtained from a completely saturated monolayer [Ulbricht et al., 2002a]. The calculation of activation energy using Redhead equation is based on the availability of a reliable pre-exponential frequency factor ν. Hence, when one employs the Redhead equation for the calculation of activation energy, one typically uses an assumed pre-exponential frequency factor $\approx 10^{12}\,\mathrm{s^{-1}}$. In general, this assumption holds true for simple diatomic or simpler polyatomic molecules, where the frequency factors are found to be of the order of $10^{12} - 10^{15}\,\mathrm{s^{-1}}$. The constant frequency factor of $k_B T/h \equiv 10^{12}\,\mathrm{s^{-1}}$ (at $T = 300\,\mathrm{K}$) is derived from the assumption

that the partition functions corresponding to transition ($q^{\ddagger}_{-1}$) and adsorbed (q_{ad}) states have the same translational, rotational, and vibrational degrees of freedom, by using the following relation [Christmann, 1991]:

$$\nu \approx \frac{k_B T}{h} \frac{q^{\ddagger}_{-1}}{q_{ad}}. \tag{3.11}$$

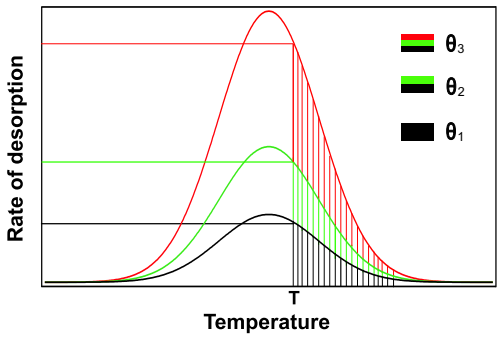

Figure 3.8.: Illustration of the Falconer-Madix analysis: Three thermal desorption traces with increasing surface coverages (red>green>black) are depicted here. At a constant temperature T, the respective desorption rates are obtained from the y-axis. The instantaneous surface coverage, $\theta(T)$, is obtained by integrating the traces between the temperature limits T and ∞, and are represented by shaded regions under each trace.

Because this assumption is generally observed for small desorbing species, the use of a fixed value of pre-exponential factors does not introduce significant error in the calculated value of activation energy. However, for bigger molecules, such as polyaromatic hydrocarbons or similar molecules, pre-exponentials can be significantly large and are reported to be as large as $10^{21}\,\mathrm{s}^{-1}$ [Ulbricht et al., 2004; Zacharia et al., 2004]. Likewise, theoretical models for thermal desorption of large long-chain alkanes from HOPG have indicated that the pre-exponential frequency factor can be considerably larger for bigger molecules in comparison to simple polyatomic species [Fichthorn and Miron, 2002]. Qualitatively, the increase in the pre-exponential factor is ascribed to the considerable differences in the degrees of freedom between the adsorbent and transition state. Therefore, when activation energy for the desorption of larger molecules, such as polyaromatic hydrocarbons, are presented in this thesis, the pre-exponentials for the peak maximum method are alternatively determined from the temperature dependence of corresponding vapor pressure data [Schlichting, 1990] (see chapter 4 for details).

The analysis of desorption spectra using the Falconer-Madix method is based on measuring the activation energy as a function of coverage at constant temperature [Falconer and Madix, 1977]. For this purpose, a series of thermal desorption traces corresponding to different initial coverages are collected, and from theses traces, the desorption rates and corresponding surface concentrations at a well-defined constant temperature are obtained. This is illustrated in Fig. 3.8, where three desorption traces (black, green and red) with increasing initial surface coverages (indicated by θ_1, θ_2 and θ_3) are depicted. The rates are obtained from the y-axis and The coverages corresponding to these rates are obtained by integrating the

curves between temperatures T and ∞, i.e.,

$$\theta = \frac{1}{\beta}\int_{T}^{\infty}\frac{d\theta}{dt}dT. \tag{3.12}$$

The respective surface coverages at temperature T in the figure are shown as the shaded region under the curves. Similarly, the rates and coverages are collected for a set of temperatures. Using pairs of coverages and desorption rates obtained from a series of TD traces, their logarithms are plotted according to the following equation:

$$\ln\left(-\frac{d\theta}{dt}\right) = \ln(\nu) + n\ln(\theta) - \frac{E_d}{k_B T}. \tag{3.13}$$

The resulting plot, a desorption rate isotherm, should be a straight line with slope n [Fig. 3.9(a)] if the activation energy of desorption is independent of surface coverage. This assumption holds true, if the data used for the construction of isotherms has the desorption trace up to only saturation coverage. Similarly, isotherms are constructed at different surface temperatures, and the intercept, I, from each of them is obtained. According to Eq. (3.13), the intercept, I, of the linear fit to the isotherms is given

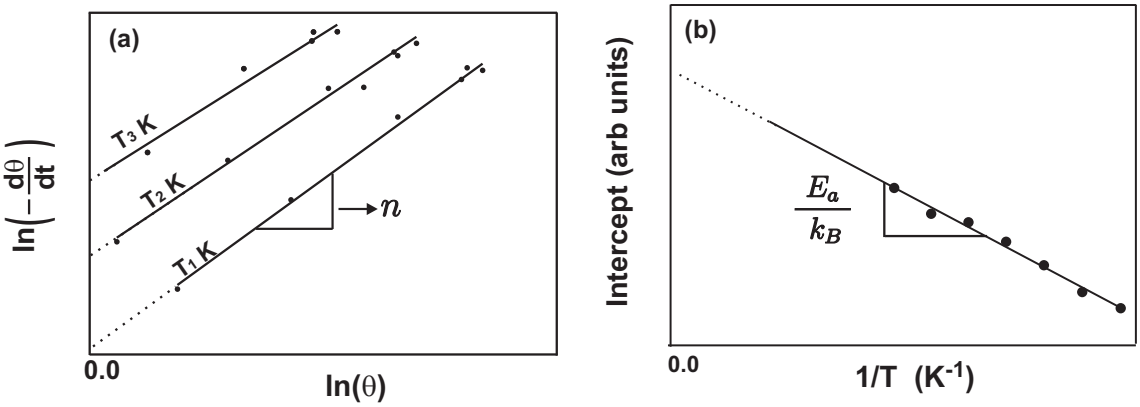

Figure 3.9.: Illustration of the analysis of isotherms and intercept plots from the Falconer-Madix method: Left panel (a) shows the plot of logarithm of desorption rate versus the logarithm of surface coverages, which is referred to as a desorption isotherm. A linear fit to isotherms is displayed along with the data. From the intercepts (broken lines) and corresponding temperatures, an intercept plot is made [right panel, (b)]. The slope and intercept of this plots are used to calculate the activation energy of desorption and the pre-exponential frequency factor.

by

$$I = \ln(\nu) - \frac{E_d}{k_B T}. \tag{3.14}$$

In order to calculate the pre-exponential frequency factor and the activation energy of desorption, the intercepts (I) are plotted versus $1/T$ [see Fig. 3.9(b)]. According

to Eq. (3.14), from the slope (E_d/k_B) and intercept ($\ln \nu$), activation energy and frequency factor are determined.

The Falconer-Madix technique is an ideal procedure to obtain kinetic and energetic parameters associated with thermal desorption without making assumptions about the frequency factor. However, since *log-log* plots are made for the analysis, the low coverage curves make disproportionately large contributions to the slope of the lines. Therefore, any discrepancies associated with pressure and temperature measurements, especially at the onset of desorption, can greatly distort the calculated values [Falconer and Madix, 1977].